Nuclear theory – nuclear astrophysics

J.W. Holt

Introduction:

The structure, phases, and dynamics of nuclear matter are crucial to understand stellar explosions, the origin of the elements, patterns in observed gravitational waves, and the composition of the densest observable matter in the universe. The appropriate tool to study strongly interacting matter at the typical scales relevant in nuclear astrophysics (well below the scale of chiral symmetry breaking $\Lambda_\chi \approx 1$ GeV) is chiral effective field theory [1-3]. In recent years, chiral effective field theory (EFT) has become a cornerstone of the modern approach to nuclear many-body dynamics that provides a systematic framework for describing realistic microphysics, such as multi-pion exchange processes and three-body forces, within a well-defined organizational hierarchy. The long and intermediate-range parts of the nuclear potential result from one- and two-pion exchange processes, while short-distance dynamics, not resolved at the wavelengths corresponding to typical nuclear Fermi momenta, are introduced as contact interactions between nucleons. Chiral effective field theory is unique in its multichannel methods for quantifying uncertainties and especially in its ability to estimate the importance of missing physics.

Chiral three-body forces at next-to-next-to-next-to-leading order

Three-nucleon forces are an indispensable ingredient for accurate few-body and many-body nuclear structure and reaction theory calculations. While the direct implementation of chiral 3N forces

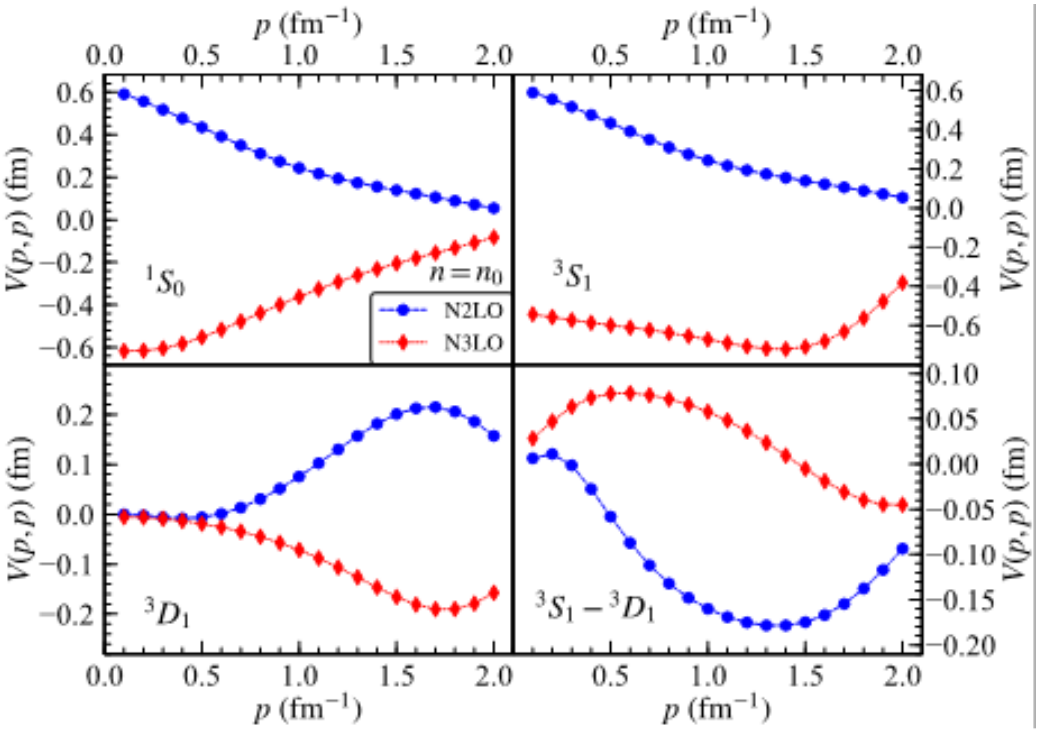

Fig. 1. Diagonal momentum-space matrix elements of the in-medium NN interaction associated with the N2LO and N3LO three-body forces in the $^1S_0$ and $^3S_1$ – $^3D_1$ partial-wave channels at saturation density in symmetric nuclear matter.

can be technically very challenging, a simpler approach is given by employing instead a medium-dependent NN interaction [4] that reflects the physics of three-body forces at the two-body normal-ordered approximation. In particular, the structure of three-body forces at next-to-next-to-next-to-leading order (N3LO) in the chiral expansion have in many cases been prohibitively challenging to implement in modern nuclear structure and reaction calculations. In recent work [5], we have constructed density-dependent nucleon-nucleon interactions from the N3LO chiral three-body force. Overall, we found that the 3N force at this order is strongly attractive in the lowest partial-wave channels. In Fig. 1 we plot the diagonal momentum-space matrix elements associated with both the total N2LO and total N3LO three-body force in the $^1S_0$ and $^3S_1 - {}^3D_1$ partial-waves in isospin-symmetric nuclear matter at saturation density. Interestingly, the N2LO and N3LO three-body force contributions have nearly equal magnitude but opposite sign. We note, however, that a relevant comparison can only be performed after the three-body N2LO low-energy constants, c_D and c_E, are refitted to the properties of three-body systems including the effects of the N3LO terms.

Adiabatic index of hot and dense matter from chiral effective field theory

Dynamical simulations of core-collapse supernovae [6-8] and neutron star mergers [9-12] require modeling of the nuclear equation of state up to densities $n \approx 5 - 10 n_0$, where $n_0 - 0.16$ fm^{-3} is the saturation density of nuclear matter, and temperatures up to 50 − 100 MeV. Such simulations are crucial for interpreting observable electromagnetic, neutrino, and gravitational wave emissions as well as understanding the origin of many heavy elements through r-process nucleosynthesis [13-15]. Presently there exist a number of equation of state tabulations derived from Skyrme mean field phenomenology and relativistic mean field models appropriate for astrophysical simulations. To explore an even wider range of parameterizations, polytropic equations of state have been coupled with an ideal gas ansatz for the thermal contribution to the pressure $p_{th} = (\Gamma_{th} - 1)\varepsilon_{th}$, where ε_{th} is the internal energy density and Γ_{th} is the so called adiabatic index. The resulting analytical equations of state have numerical advantages over tabulations and allow for a more thorough exploration of the correlations among bulk neutron star properties, features of gravitational wave signals, and properties of the equation of state. In particular, thermal effects have been shown to modify the dominant peak frequency and intensity of the post-merger gravitational wave signal [11] and lead to a delay in the remnant collapse time to a black hole [11].

Previous numerical simulations of neutron star mergers have employed a constant value of the thermal index, and recently we have provided [16] a general parameterization for Γ_{th} based on finite-temperature calculations of the equation of state from microscopic chiral effective field theory. In Fig. 2 we show uncertainties in the density- and temperature-dependent adiabatic index obtained from mean field models constrained by chiral effective field theory. We find in particular that microscopic chiral effective field theory yields a consistently larger adiabatic index compared to traditional Skyrme force models and especially relativistic mean field models.

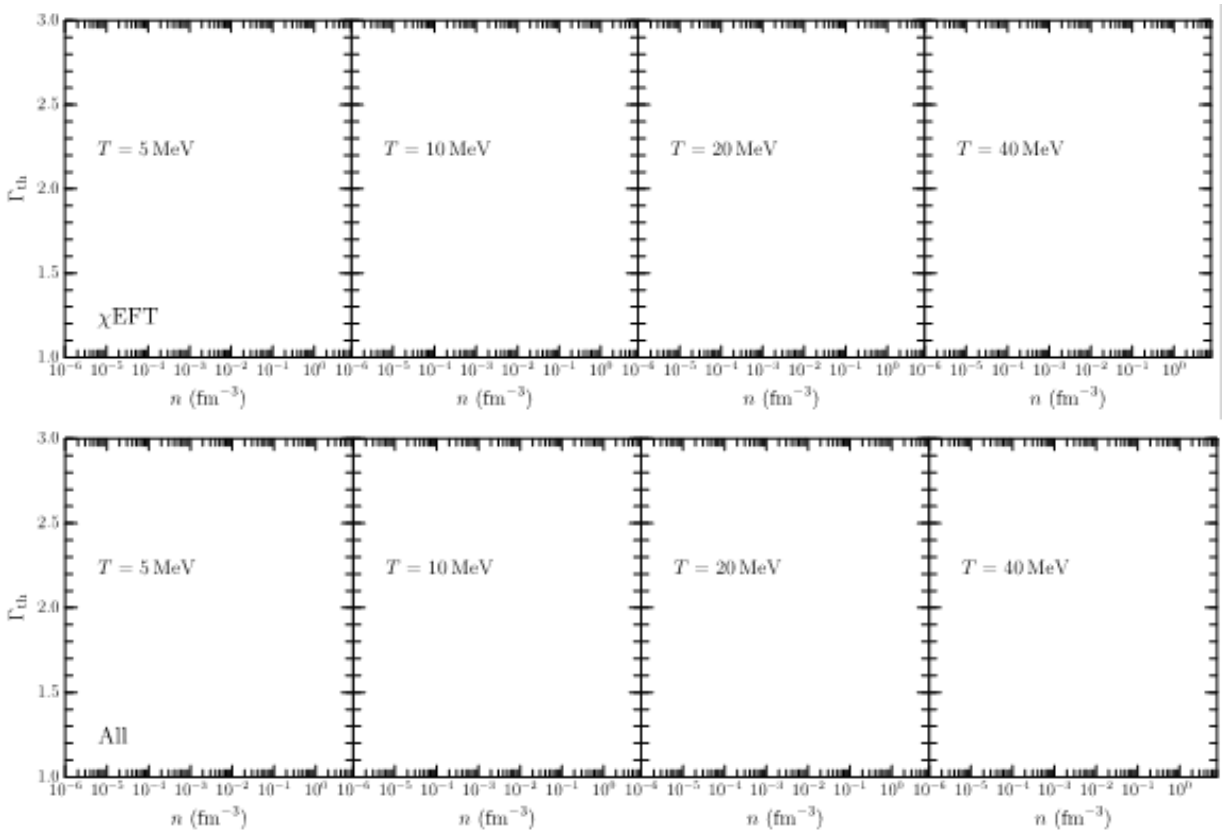

Fig. 2. Adiabatic index confidence intervals of $\pm 1\sigma$ and $\pm 2\sigma$ obtained from Skyrme and Relativistic Mean Field models ("ALL") as well as models constrained by chiral effective field theory ("χEFT").

Neutron-nucleus optical potentials from chiral two- and three-body forces

Numerical simulations of r-process nucleosynthesis are essential for identifying the astrophysical site of the r-process, the primary candidates being the wind-driven ejecta from accretion disks surrounding binary neutron-star mergers or collapsars as well as the neutrino-driven winds of core-collapse supernovae. Neutron-capture rates on exotic neutron-rich isotopes are particularly important during the non-equilibrium freeze-out phase of r-process nucleosynthesis, but direct experimental studies at rare-isotope facilities remain unfeasible. The large uncertainties in these capture rates, due in part to difficulties in extrapolating phenomenological optical model potentials far from the valley of stability, limit the precision of predicted heavy-element abundances. Previously we have computed proton-nucleus optical potentials [17] by combining the improved local density approximation with chiral effective field theory calculations of the nucleon self energy in homogeneous nuclear matter. Differential elastic scattering cross sections on calcium isotopes were found to be in quite good agreement with experimental data for projectile energies up to 150 MeV.

More recently, we have computed also neutron-nucleus optical potentials [18] for calcium isotope targets. Given the important role of the Coulomb potential at small scattering angles in the case of proton elastic scattering, testing our approach with a neutron projectile was a nontrivial extension. We also computed for the first time in our formalism vector analyzing powers. This is an important test of the quality of our spin-orbit optical potential that was not benchmarked in our previous calculations. The real

spin-orbit optical potential was constructed within the density matrix expansion [19] from consistent chiral two-body and three-body forces. In Fig. 3 we show the analyzing powers for n-40Ca elastic scattering at projectile energies E = 11.9, 16.9 MeV. Results from the chiral optical potential are given by the blue bands obtained by varying the smearing length in the improved local density approximation. We find quite good agreement with our results and experimental data (shown as red dots with error bars in Fig. 3) and the results from the Koning-Delaroche phenomenological optical potential [20] (green dashed curves).

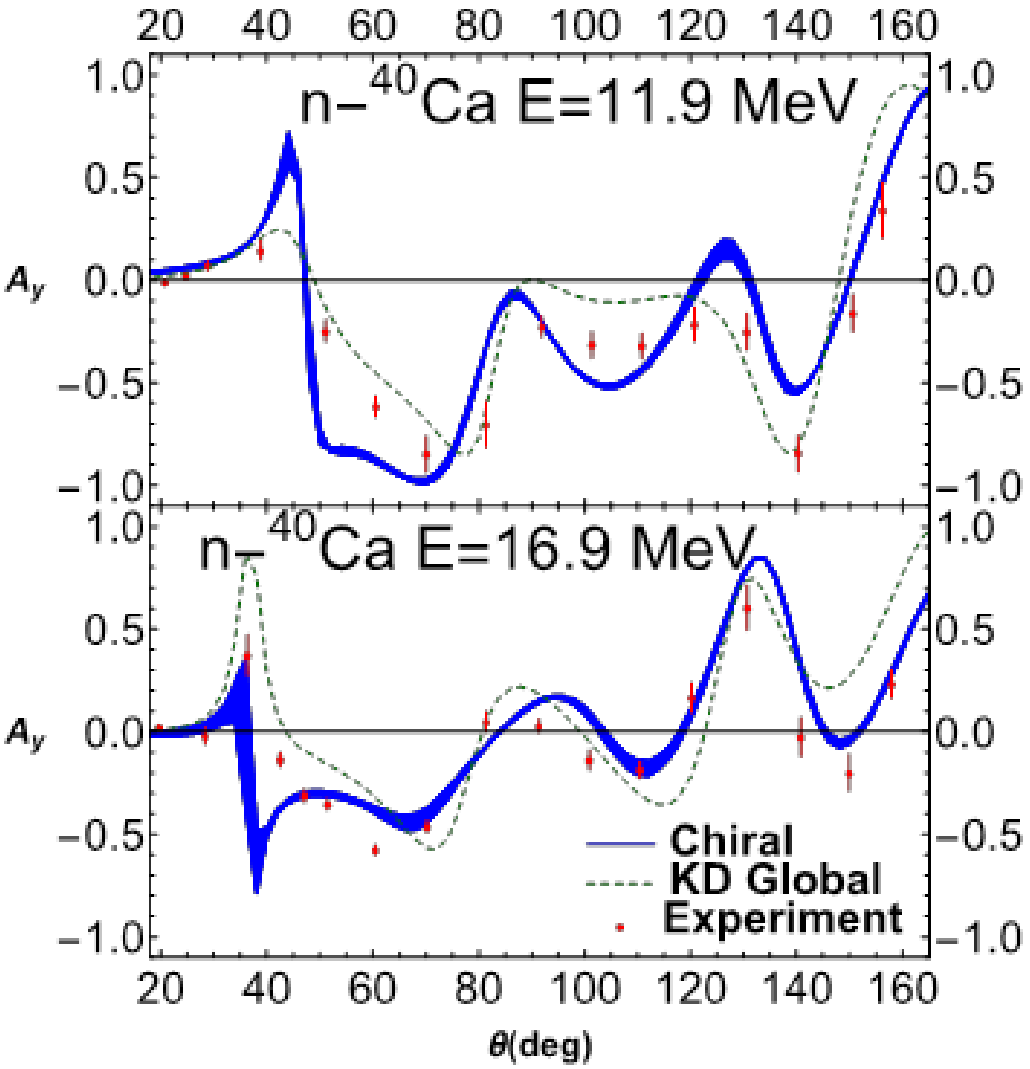

Fig. 3. Vector analyzing powers for elastic n-40Ca scattering at projectile energies E = 11.9, 16.9 MeV. Results from the chiral optical potential are given by the blue bands, while those from the Koning-Delaroche phenomenological optical potential are given by the green dashed curves. Experimental data are represented by red circles with error bars.

[1] S. Weinberg, Physica A **96**, 327 (1979).

[2] E. Epelbaum, H.-W. Hammer, and U.-G. Meissner, Rev. Mod. Phys. **81**, 1773 (2009).

[3] R. Machleidt and D.R. Entem, Phys. Rep. **503**, 1 (2011).

[4] J.W. Holt, N. Kaiser, and W. Weise, Phys. Rev. C **79**, 054331 (2009).
[5] J.W. Holt, M. Kawaguchi, and N. Kaiser, Front. Phys. **8**, 100 (2020).
[6] H.-T. Janka, K. Langanke, A. Marek, G. Martínez-Pinedo, and B. Müller, Phys. Rep. **442**, 38 (2007).
[7] C.D. Ott, E. Abdikamalov, P. Mösta, R. Haas, S. Drasco, E.P. O'Connor, C. Reisswig, C.A. Meakin, and E. Schnetter, Astrophys. J. **786**, 115 (2013).
[8] T. Melson, H.-T. Janka, R. Bollig, F. Hanke, A. Marek, and B. Müller, Astrophys. J. **808**, L42 (2015).
[9] M. Ruffert and H.T. Janka, Astron. Astrophys. **338**, 535 (1998).
[10] R. Oechslin, H.-T. Janka, and A. Marek, Astron. Astrophys. **467**, 395 (2007).
[11] A. Bauswein, H.-T. Janka, and R. Oechslin, Phys. Rev. D **82**, 084043 (2010).
[12] D. Kasen, B. Metzger, J. Barnes, E. Quataert, and E. Ramirez-Ruiz, Nature **551**, 80 EP (2017).
[13] J.M. Lattimer and D.N. Schramm, Astrophys. J. **192**, L145 (1974).
[14] F.-K. Thielemann, M. Eichler, I. Panov, and B. Wehmeyer, Ann. Rev. Nucl. Part. Sci. **67**, 253 (2017).
[15] D. Radice, A. Perego, K. Hotokezaka, S.A. Fromm, S. Bernuzzi, and L.F. Roberts, Astrophys. J. **869**, 130 (2018).
[16] Y. Lim and J.W. Holt, arXiv:1909.09089.
[17] T.R. Whitehead, Y. Lim, and J.W. Holt, Phys. Rev. C **100**, 014601 (2019).
[18] T.R. Whitehead, Y. Lim, and J.W. Holt, Phys. Rev. C **101**, 064613 (2020).
[19] J.W. Holt, N. Kaiser, and W. Weise, Eur. Phys. J. A **47**, 128 (2011).
[20] A.J. Koning and J.P. Delaroche, Nucl. Phys. **A713**, 231 (2003).